Discussion of a physical optics method and its application to absorbing smooth and slightly rough hexagonal prisms

E. Hesse[a], L. Taylor[a], C.T. Collier[a], A. Penttilä[b], T. Nousiainen[c], Z. Ulanowski[a]

[a]*University of Hertfordshire, Centre for Atmospheric and Climate Physics Research, Hatfield, Hertfordshire AL10 9AB, UK*

[b]*Department of Physics, P.O. Box 64, University of Helsinki, FI-00014, Finland*

[c]*Finnish Meteorological Institute, FI-00101 Helsinki, Finland*

Keywords: light scattering, diffraction, absorbing facetted particle, rough particle

Abstract

Three different mathematical solutions of a physical optics model for far field diffraction by an aperture due to Karczewski and Wolf are discussed. Only one of them properly describes diffraction *by an aperture* and can, by applying Babinet's principle, be used to model diffraction by the corresponding plane obstacle, and *by further approximation*, diffraction *by a particle*. Studying absorbing scatterers allows a closer investigation of the external diffraction component because transmission is negligible. The physical optics model has been improved on two aspects: (i) To apply the diffraction model based on two-dimensional apertures more accurately to three-dimensional objects, a size parameter dependent volume obliquity factor is introduced, thus reducing the slightly overestimated side scattering computed for three-dimensional objects. (ii) To compensate simplifications in the underlying physical optics diffraction model for two-dimensional apertures [26] a size parameter dependent cross polarisation factor is implemented. It improves cross polarisation for diffraction and reflection by small particle facets. 2D patterns of P_{11}, $-P_{12}/P_{11}$ and P_{22}/P_{11} and their azimuthal averages for slightly rough absorbing hexagonal prisms in fixed orientation are obtained and compared with results from the discrete dipole approximation. For particle orientations where shadowing is not negligible, improved phase functions are obtained by using a new method where the incident beam is divided into sub-beams with small triangular cross sections. The intersection points of the three sub-beam edges with the prism define the vertices of a triangle, which is treated by the beam tracer as an incidence-facing facet. This ensures that incident facing but shadowed crystal facets or regions thereof do not contribute to the phase functions. The method captures much of the fine detail contained in 2D scattering patterns obtained with DDA. This is important as speckle can be used for characterizing the size and roughness of small particles such as ice crystals.

1. Introduction

The Earth–atmosphere radiation balance is influenced by the scattering and absorption of solar radiation by airborne particles such as ice crystals [1] and Saharan dust [2]. For radiative transfer computations a more realistic parameterisation of the bulk single scattering properties (phase functions, volume extinction coefficients, single scattering albedos etc.) of these particles is required. To achieve this, a detailed knowledge of particle shapes, sizes and composition is essential [1]. Imaging methods (for a discussion of methods and instruments see e.g. [3]) are widely used for particle characterisation, however for small particles optical aberrations and constrained depth of field restrict the quality of the information obtainable. Such constraints do not apply to instruments such as the Small Ice Detector (SID) [4,5], which acquire far field scattering patterns. For complex or rough particles, the presence of two-dimensional speckle can be used to derive both particle size [6] and roughness [5]. However, obtaining quantitative morphological data by inversion of the patterns can be very challenging. Therefore, the creation of databases of two-dimensional (2D) scattering patterns of known particle morphologies is extremely useful for particle characterization. Exact methods such as T-matrix [7] and semi-exact methods like the finite difference time domain (FDTD) method [8] and the discrete dipole approximation (DDA) [9,35] can be used for computations of light-scattering properties for non-axisymmetric particles. Those methods that are most versatile and can be applied to arbitrary particle morphologies are computationally most demanding and cannot be used if the objects are much larger than the wavelength. For single orientations the computational burden is strongly reduced, allowing application to larger sizes, as is done here with the DDA method.

Approximate methods, such as the geometric optics approximation or physical optics have to be used for scatterers much larger than the wavelength of radiation. In the classical geometric optics approximation, scattered light is divided into two parts, firstly light reflected or transmitted by the scatterer, and secondly externally diffracted light. Diffraction of reflected and refracted light is neglected. Improved methods including diffraction of the ray-tracing component have been presented e.g. in [10-13]. A volume integral method, which avoids the separation between externally diffracted and reflected/transmitted light, has also been presented [14-16]. Nevertheless, computational methods that calculate the ray-tracing and diffraction contributions separately, are still widely used. In many applications, e.g. [17-19], external diffraction is approximated by Fraunhofer diffraction on the projected cross section, applying Babinet's principle. Macke et al. [17] approximated diffraction by polyhedral particles as diffraction by polygonal apertures corresponding to the projected particle cross section, using the Kirchhoff approximation. The method to calculate diffraction by a circular aperture at oblique incidence by means of the Kirchhoff approximation ([20], chapter 10.9) has recently been extended to oblique incidence on polygonal apertures and applied to compute 2D scattering patterns and phase function of absorbing [21,22] and transparent [23] facetted particles in fixed orientation. (In geometric optics 2D scattering patterns for fixed particle orientations do not show the familiar scattering arcs but only scattering points. This is due to the singular directions of rays or beams reflected from faceted particles, see e.g. [24]). The method [23] has been applied to interpret two-dimensional reflections of a lidar beam by ice crystals [25]. In [22, 23] we applied the approximate vector method described by Karczewski and Wolf [26,27] to model light scattering by absorbing facetted particles. This method expresses electric and magnetic fields using electric and magnetic Hertz vectors. Karczewski and Wolf also proposed alternative approximations, expressing electric and magnetic fields using either electric or magnetic Hertz vectors alone. These alternative solutions have been discussed in the current literature [28]. Aiming for clarification, we investigate these alternative solutions and in particular the high backscattering reported in [28] at the beginning of section 2.1 of this paper. As an example, diffraction by a hexagonal prism is computed, making use of Babinet's principle.

Here, our main interest is in modelling 2D scattering patterns, i.e. azimuthally resolved phase functions, of single particles. Studying absorbing scatterers allows a closer investigation of the external diffraction component because transmission is negligible. In [21,22] we found by comparison with DDA, which is a semi-exact method, that side scattering was slightly too high in our beam tracing results. It was conjectured that this was due to modelling Kirchhoff diffraction by individual facets of the scatterer, disregarding the fact that they were part of a three-dimensional object. The contribution of edge effects have been discussed e.g. in [29]. In the second part of section 2.1 we introduce a volume obliquity factor to allay this problem. Comparisons of the phase function and P_{12} phase matrix element with DDA results are used to find this parameter for a smooth hexagonal prism. The P_{22} phase matrix element is also improved when applying the volume obliquity factor, however cross polarisation is still too high. To alleviate this, a cross polarisation factor is introduced.

Particle roughness has been reported to alter the scattering properties of ice crystals, in some cases even dramatically [5,30,31,41]. To model deviations from perfect hexagonal particle symmetry, Macke et al. [17] had introduced random tilt of facets. Yang and Liou applied a similar method to approximate polyhedral facets with Gaussian roughness [32]. Furthermore, the approach [17] has been used to simulate rough surfaces after including Weibull statistics [30] or a normal distribution for the random tilt [33], respectively. The random tilt method has also been implemented in the Improved Geometric Optics Method (IGOM) [33,34]. However, the random tilt method does not model continuous surfaces. Results for a version of IGOM for randomly aligned hexagonal prisms with geometrically defined roughened surfaces have been published by Liu et al. [33]. In order to compute reflection by dielectric particles, diffraction of the reflected component determined from the Fresnel equations has to be calculated [21-23]. The case of high absorption is particularly suitable for studying how the three-dimensional nature of the scattering object affects external diffraction. Here we compute scattering by an absorbing, slightly rough dielectric prism. Accurate phase treatment is essential.

The remainder of this article is structured as follows: In section 2 we describe our method and results. A summary describing the applied diffraction model is given in section 2.1. In its first subsection we investigate different boundary conditions proposed by Karczewski and Wolf [26] in order to decide which of them should be used for modelling scattering by dielectric particles. In the following subsection the applicability of our diffraction model based on substituting two-dimensional apertures for three-dimensional objects is investigated for the case of an absorbing hexagonal prism for different size parameters and orientations by comparing the scattering phase matrix elements P_{11}, P_{11}/P_{12} and P_{22}/P_{11} with DDA results. A size-dependent volume obliquity factor is introduced to better approximate side-scattering for external diffraction. An also size-dependent cross polarisation factor is introduced for both external diffraction and reflection, to approximate depolarisation more accurately, especially for small size parameters. In section 2.2 the model is applied to slightly rough absorbing prisms and the results are compared with DDA [35] for fixed orientations. Conclusions are given in section 3.

2. Method and Results

The method used here combines geometric optics beam tracing with diffraction. Externally reflected beams and beams refracted out of the particle undergo diffraction at the respective facet. For the strongly absorbing particles investigated here, only external reflection is considered. External diffraction is computed by applying Babinet's principle to beam-facing facets. The amplitude matrix and corresponding phase matrix for each scattering angle are calculated. The diffraction model used for calculating external diffraction and diffraction of reflected beams is discussed in section 2.1. Firstly, alternative options for boundary conditions described by Karczewski and Wolf [26] are

considered. Secondly, the effect of three-dimensionality of the facetted object on external diffraction is investigated for the example of a hexagonal prism. In section 2.2 the model is applied to compute 2D scattering patterns of a strongly absorbing hexagonal prism with slightly rough surface.

2.1 The diffraction model

In [22] we used the method described by Karczewski and Wolf [26] to compute far-field diffraction patterns for diffraction of a plane wave by an aperture. The authors of [26] imposed approximate boundary conditions of the Kirchhoff type (i.e. continuity of the tangential components of the electric field **E** and the magnetic field **H**) and assumed that the diffracted field obeys the vectorial form of the Sommerfeld radiation condition at infinity in the half-space into which the field is propagated.

They showed that the electric field at a point *P* in the Fraunhofer region is given by [26]

$$\mathbf{E}(P) = \hat{\mathbf{k}} \times (\mathbf{F} \times \mathbf{E_0}) + \mu_0 c\left[(\mathbf{F} \times \mathbf{H_0}) - \hat{\mathbf{k}} \cdot (\mathbf{F} \times \mathbf{H_0})\hat{\mathbf{k}}\right] \tag{1}$$

where $\mathbf{F} = \frac{ik_0}{4\pi}\frac{\exp(ik_0 r)}{r}\hat{\mathbf{n}} \iint_A \exp\left[ik_0\left(\hat{\mathbf{K}} - \hat{\mathbf{k}}\right) \cdot \mathbf{R}\right] dS = F\hat{\mathbf{n}}$ (2)

is the integral over the aperture (Fig. 1). Here, k_0 is the wave number, $\hat{\mathbf{K}}$ is the unit vector in direction of propagation of the field incident at an angle α to the surface normal (*z*' axis). The plane of incidence is chosen to be the *x*'*z*' plane, which acts as a reference plane. $\mathbf{E_0}$ and $\mathbf{H_0}$ are amplitude vectors of the incident field, $\hat{\mathbf{k}}$ is the unit vector pointing from the centre of the aperture towards *P* and $\mathbf{R}$ is the vector pointing from the origin of the coordinate system to the aperture point under consideration. The surface integral in Eq. (2) can be evaluated using Green's theorem:

$$\begin{aligned}\int_S e^{ik[x'(\sin\alpha+\cos\varphi'\sin\theta')+y'\sin\varphi'\sin\theta'+z'(\cos\alpha+\cos\theta')]}dx'dy' \\ = -\oint_S \frac{e^{ik[x'(\sin\alpha+\cos\varphi'\sin\theta')+y'\sin\varphi'\sin\theta'+z'(\cos\alpha+\cos\theta')]}}{2ik\sin\varphi'\sin\theta'}dx' \\ + \oint_S \frac{e^{ik[x'(\sin\alpha+\cos\varphi'\sin\theta')+y'\sin\varphi'\sin\theta'+z'(\cos\alpha+\cos\theta')]}}{2ik(\sin\alpha+\cos\varphi'\sin\theta')}dy'\end{aligned} \tag{3}$$

Note that before applying these equations to compute diffraction by a facet of a particle centred at the origin, the coordinate system needs to be rotated by a rotation matrix $\mathbf{R_0}$ [43] given in the appendix, so that the facet becomes aligned parallel to the *x*'*y*' plane. In general, its *z*' coordinate will be nonzero. Therefore, the exponents of the phase terms in the line integrals in Eq. (3) contain a *z*' component. This is different from the corresponding equations in [20] and [17, 36], where diffraction on the projected cross section of a particle was considered. This is especially important for particles with rough surfaces, which are modelled as an ensemble of small facets tilted against each other (see section 2.2), and where small phase differences between waves diffracted by neighbouring facets will affect the scattering pattern.

Both the incident and the diffracted field can be represented as a vector sum of one component parallel to this plane and one component perpendicular to the first vector and to the propagation vector of the wave considered. For this purpose we choose sets of unit vectors [$\hat{\mathbf{L}}$, $\hat{\mathbf{M}}$] and [$\hat{\mathbf{l}}$, $\hat{\mathbf{m}}$], where $\hat{\mathbf{L}}$ and $\hat{\mathbf{l}}$ are positioned in the reference plane, and $\hat{\mathbf{M}} = \hat{\mathbf{L}} \times \hat{\mathbf{K}}$, $\hat{\mathbf{m}} = \hat{\mathbf{l}} \times \hat{\mathbf{k}}$.

Karczewski and Wolf expressed the scattered field $\mathbf{E}^{(e,m)}$ in components parallel and perpendicular to the incidence plane $\begin{bmatrix} E_l \\ E_m \end{bmatrix} = \mathbf{D} \begin{bmatrix} E_{0L} \\ E_{0M} \end{bmatrix}$ where $\mathbf{D}$ is the amplitude diffraction matrix [26,22].

In the next step, by multiplying with a rotation matrix $\mathbf{R_1}$ the matrix $\mathbf{D}$ is rotated around the vector $\hat{\mathbf{k}}$ into the scattering plane containing the incidence vector $\hat{\mathbf{K}}$. Finally, the pre-multiplication matrix $\mathbf{R_p}$ [12,22] is included to rotate the amplitude matrix of the incident beam around its propagation vector into the plane containing $\hat{\mathbf{k}}$. Therefore, the amplitude matrix describing external diffraction by the particle into direction $\hat{\mathbf{k}}$ can be written as $\mathbf{S_D} = \mathbf{R_1.D.R_0.R_p}$. Similarly, the amplitude phase matrix describing external reflection into direction $\hat{\mathbf{k}}$ by the particle can be written as $\mathbf{S_R} = \mathbf{R_1.D}.\boldsymbol{\mathcal{R}}.\mathbf{R_0.R_p}$, where $\boldsymbol{\mathcal{R}}$ is the generalised Fresnel amplitude reflection matrix [22].

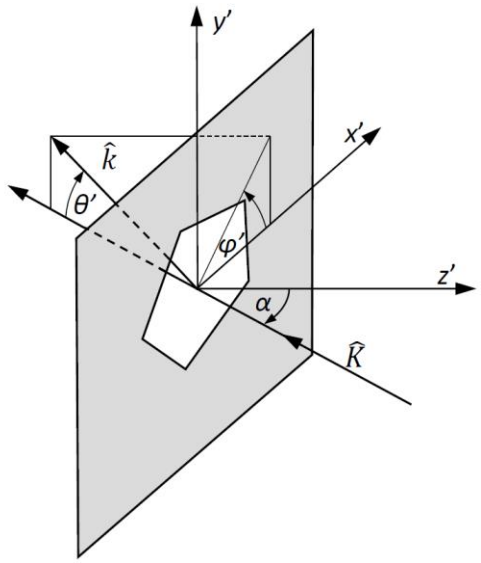

Fig. 1. Diffraction by an aperture: oblique incidence.

Discussion of boundary conditions proposed in [26]

The first and second addend at the right hand side of eq. (1) are the electric field components derived from magnetic and electric Hertz potentials, respectively. This is indicated by superscripts (*m*) and (*e*) in Eqs. (4a) and (4b), respectively.

$$\mathbf{E}^{(m)}(P) = \hat{\mathbf{k}} \times (\mathbf{F} \times \mathbf{E_0}) \tag{4a}$$

$$\mathbf{E}^{(e)}(P) = \mu_0 c\left[(\mathbf{F} \times \mathbf{H_0}) - \hat{\mathbf{k}} \cdot (\mathbf{F} \times \mathbf{H_0})\hat{\mathbf{k}}\right] \tag{4b}$$

Eq. (4a) involves only the tangential component of the electric field on the aperture plane, whereas Eq. (4b) involves only the tangential component of the magnetic field on the aperture plane. Karczewski and Wolf called the method based on Eq. (1) the (*e*,*m*) theory [26]. The corresponding diffraction matrix D is given in the appendix. Referring to [37], Karczewski and Wolf stated that consistent solutions can also be obtained when imposing the boundary conditions and Sommerfeld radiation condition on $\mathbf{E}^{(m)}$ or $\mathbf{E}^{(e)}$ only, calling these approaches the (*m*) theory and the (*e*) theory, respectively. These results [26] are also discussed in [28,38]. In particular, the authors of [11] and [28] have shown that the (*e*,*m*) theory is equivalent to the surface integral equation, which is derived from the Maxwell equations and can be extended to all scattering directions without any truncation.

In [22] we applied the (*e*,*m*) theory [26] to calculate external diffraction by an isometric hexagonal prism. Seeking clarification on the applicability of the (*e*), (*m*) and (*e*,*m*) theories, we now investigate these three approaches for the same case. Prism height, edge length of the basal facets and wavelength are 10 µm, 5 µm and 0.5 µm, respectively. As an application of Babinet's principle, the incidence-facing facets are treated as apertures. Fig. 2 shows the results for the scattered intensity (left panel) and degree of linear polarisation (DLP) $-P_{12}/P_{11}$, where P_{11} and P_{12} are elements of the phase matrix (right panel) vs. scattering angle for the (*e*,*m*), (*e*) and (*m*) approaches, and additionally for the solution $\mathbf{E}^{(m)}(P) - \mathbf{E}^{(e)}(P)$, which we abbreviate as (-*e*,*m*). The angular intensity distributions obtained by the (*e*,*m*), (*e*) and (*m*) methods have a strong peak in the direct forward direction representing external diffraction, but both the (*e*) and (*m*) solutions also contain strong reflection components. These reflection components correspond to a perfectly reflecting particle. The identical (-*e*,*m*) and (*e*,-*m*) solutions represent reflection from the three beam-facing facets. For comparison, we show the phase function for a hexagonal prism composed of silver (refractive index 0.05+3.13i at 500nm [39]) computed by combining the (*e*,*m*) solutions for external diffraction and reflection as demonstrated in [22].

Our results are related to findings of Konoshonkin et al. [28], who applied the (*e*,*m*), (*m*) and (*e*) approaches to compute diffraction by a hexagonal aperture for the cases of perpendicular and oblique incidence and reported a 'false maximum as a mirroring of the true maximum'. They concluded that (*e*) and (*m*) solutions have to be truncated at the plane containing the aperture. Our results show essentially the same phenomenon, however we interpret them slightly differently and conclude that the (*e*) and (*m*) solutions are directly applicable to obtaining the phase functions of perfectly conducting particles (i.e. they do not require computing diffraction of the reflected beam in a separate step). This can be explained by the choice of boundary conditions: the continuity of the tangential **E** or **H** field as required for free space is guaranteed, whereas the other respective component is disregarded, which for the (*e*) case in effect corresponds to the boundary condition for a conductor, where the tangential component of **E** is zero [40].

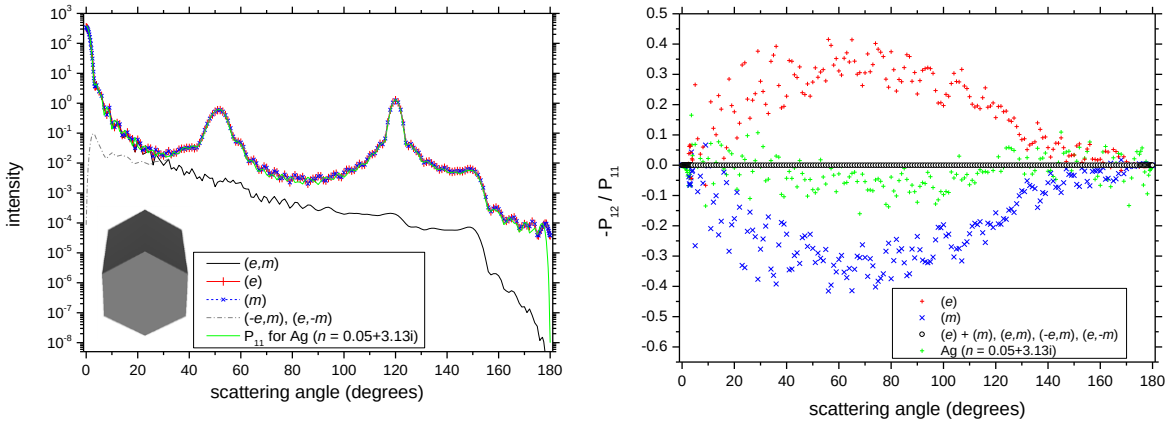

Fig. 2. Azimuthally averaged intensity (left panel) and $-P_{12}/P_{11}$ (right panel) for the (*e*,*m*), (e), (*m*), (-*e*,*m*) and (*e*,-*m*) external diffraction solutions and combined external diffraction (D) and reflection (R), R-D (the (e,m) solution is used for D) for silver (*n* = 0.05+3.13i) at wavelength 500 nm. The crystal orientation is given in the inset of the left panel (light incidence is perpendicular to the page).

The right panel in Fig. 2 shows the computed DLP for the silver prism obtained from the (*e*,*m*), (*e*), (*m*), (-*e*,*m*) and (*e*,-*m*) methods and the result for (*e*)+(*m*). The mirrored signs for the (*e*) and (*m*) solutions mean, similarly to findings in [28], that DLP values are only realistic in the regions close to the direct forward and backscattering directions and GO reflection peaks (visible in 2D patterns not shown here), where the DLP approaches zero. We conclude that the (*e*) and (*m*)

solutions, although valid from a mathematical point of view, do not fulfil the other essential requirement stated by di Franca [37], that the electric/magnetic fields really exist in the aperture plane. Therefore, for modelling scattering by *dielectric* particles only the (*e*,*m*) solution should be used: part of the light will be refracted into the particle, therefore external reflection will be lower than for a conductor and its diffraction must be calculated separately in the method discussed here.

Approximating diffraction by a three-dimensional facetted particle using the plane aperture diffraction model

Reflection and external diffraction by strongly absorbing dielectric prisms have been discussed in detail in [22,23]. For reflection off a dielectric facetted particle, the Fresnel amplitude reflection coefficient for each incidence-facing facet is calculated and in the next step diffraction of the reflected beam is computed as diffraction by a reflecting polygon in the same way as described in section 2.1. However, $\widehat{\mathbf{K}}$, $\mathbf{E_0}$ and $\mathbf{H_0}$ are here the direction of propagation of the reflected ray according to geometric optics and its amplitude vectors. Diffraction amplitude matrices are subtracted from reflection amplitude matrices [22]. Due to the high imaginary part of the refractive index, transmission through the crystal and higher order beam interactions are assumed to be negligible.

Although overall agreement of phase functions with DDA was good, it was initially found that modelled sideward diffraction was slightly too high. This is a phenomenon linked to applying physical optics approximations. It has been discussed e.g. in [42], [12], and can be found in results reported in the literature, e.g. [16]. Unsurprisingly, it is also visible in results obtained from classical geometric optics [17] combining ray-tracing with Kirchhoff diffraction at the projected cross section (see also discussion of Fig. 4 below). It is most likely due to computing diffraction at thin plane obstacles, disregarding the three-dimensional nature of the scattering particle: to propagate into certain far field directions, the diffracted radiation would need to 'move around' the particle. In the following, the amplitude matrix obtained for external diffraction is multiplied by a size-parameter-and-scattering-angle-dependent volume obliquity factor $VOF(X,\theta)$ in order to improve the scattering patterns and phase functions obtained from our scattering model. In the approximation used here, the azimuthal variation of *VOF* is not considered. Note that *VOF* is different from the obliquity factor commonly used in scalar diffraction theory (e.g. [20], chapter 10.5). Decrease of scattering towards the backscattering direction is already inherent in the vector diffraction model [26,22]). As an example, light scattering by a smooth hexagonal prism of refractive index n = 1.31 + 0.1i with an edge length a of the basal facets and a prism height $2a$ is investigated for size parameters $X = 2\pi a/\lambda$ = 20, 40, 62 and 100. Particle orientations were chosen in such a way that there are no reflection peaks in the side scattering region: For the DDA calculations, the crystal is kept fixed with its long axis parallel to the *z*-axis and the incident beam, which propagates originally into –*z*, is rotated. The beam is first rotated about the *y* axis and this is followed by a rotation about the *z* axis. We describe the resulting set up as being 'off A×B' where A and B are the rotation angles. Schematics of the three investigated particle orientations can be seen on top of Fig. 4 (a). For the volume obliquity factor a fit function

$$VOF(X,\theta) = \cos^{m(X)}(\theta) \tag{5a}$$

was used. Best fits were obtained using the method of least squares. The parameter $m(X)$ was obtained separately for the investigated size parameters and orientations, see Fig. 3(a). The figure shows some variation of m with particle orientation for the same size parameter: m is largest for 'off 30˚×0˚', where two facet normals are perpendicular to the incidence direction, and smallest for 'off 30˚×30˚', where all prism facets are noticeably tilted with respect to the incidence direction. For size parameter 62 four additional orientations, 'off 30˚×5˚', 'off 30˚×10˚', 'off 30˚×20˚' and 'off 30˚×25˚' were investigated. It was found that m decreases from 'off 30˚×0˚' to 'off 30˚×20˚' with the largest decrease between 'off 30˚×15˚' and 'off 30˚×20˚'. The value of m does not noticeably change

between ‘off 30˚×20˚’ and ‘off 30˚×30˚’. Next, averages of $m(X)$ over the investigated orientations were taken for each size parameter. The following fit function was obtained:

$$m(X) = -15.085 \cdot \exp(-X/240.448) + 13.916. \quad (5b)$$

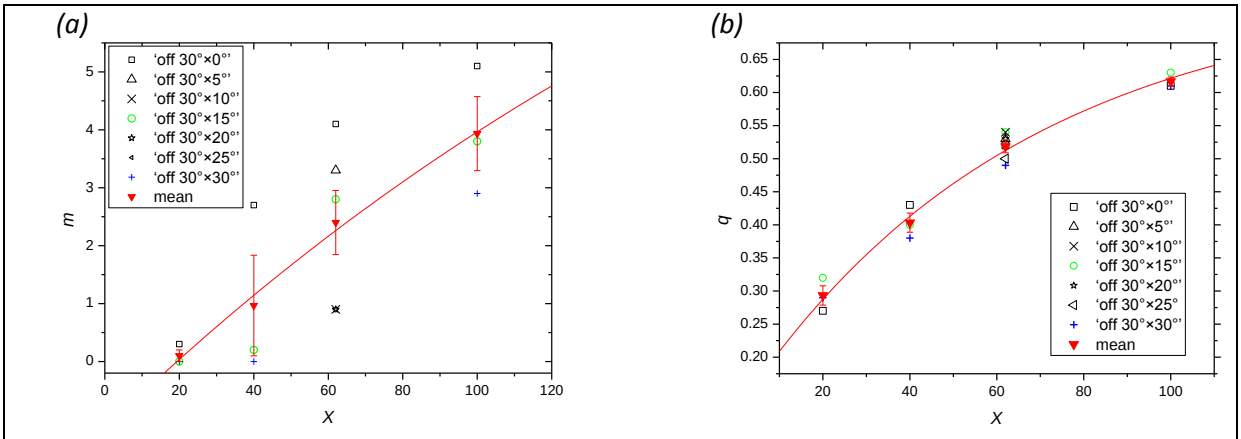

Fig. 3. (a) Exponent *m* of volume obliquity factor *VOF* obtained vs. size parameter *X* for the investigated particle orientations. (b) Factor *q* of cross polarisation obliquity factor *CPF* obtained vs. size parameter *X* for the investigated particle orientations.

Figs. 4(a) and (b) show comparisons with DDA [35] (black lines) of beam tracer results for phase functions and $-P_{12}/P_{11}$ for the investigated size parameters and orientations, respectively. In the side scattering region, the classical geometric optics [17] results (gray lines, shown for size parameter 100) are very similar to the beam tracer results without *VOF*. This is due to the fact, that both diffraction algorithms are based on Kirchhoff diffraction theory (scalar and vector approximation for diffraction on projected cross section in [17] and the beam tracer, respectively). The *VOF* has not been applied to reflection since the reflected beam will point away from the particle, therefore obstruction of diffracted components by a convex particle will occur less.

Due to the values of the Fresnel reflection coefficients, $-P_{12} / P_{11}$ is expected to be high at external reflection peaks. These are located at 51˚ and 120˚ for ‘off 30˚×0˚’, at 15˚ (shoulder), 43˚, 56.5˚ and 120˚ for ‘off 30˚×15˚’, and at 28˚, 60˚ and 120˚ for ‘off 30˚×30˚’ (see also peaks in classical geometric optics graphs). The peak at 120˚ is due to reflection at the basal facet, whereas the other peaks are due to reflections at prism facets. Correspondingly, the graphs computed with the beam tracer without applying the *VOF* (green lines) show two broad maxima with centre between 50˚ and 60˚, and 110˚ and 120˚, respectively. The strongly undulating DDA results for size parameter 20 show such maxima, too. However, the DDA results for larger size parameters show a broad maximum with centre around 95° corresponding to a broad minimum of the phase function, and a shoulder around 60°. The broad maximum is due to diffracted contributions from the reflection peaks coinciding with very low contributions from the essentially unpolarised external diffraction. The phase function has a wide minimum around 90˚, but light scattered into this region is strongly linearly polarised. The difference between the beam tracer result without the application of *VOF* and the result from the reference method, DDA, is largest for the orientation ‘off 30˚×0˚’. In this orientation two prism facets are parallel to the direction of incidence. It seems evident, that external diffraction is obstructed most for this orientation (and it might be obstructed even more for alignment of the prism axis parallel to the incidence direction). Consequently, the *VOF* is largest for this orientation for all investigated size

parameters, although the difference between orientations is small for size parameter 20. The use of orientation averaged rather than orientation-specific *VOF* can worsen agreement with DDA for individual orientations, in particular around size parameter 40. One should note that the high $-P_{12}/P_{11}$ values in side scattering are specific for the high absorption case and therefore provide a strict test case. For transparent particles reflection and transmission peaks will contribute to the side scattering region, resulting in lower absolute values of $-P_{12}/P_{11}$ (see e.g. [41]). Applying the *VOF* significantly improves the beam tracer results for $-P_{12}/P_{11}$ for size parameters 62 and 100. At size parameter 20 the *VOF* has only minor effect on scattering, since the particle is too small to obstruct the diffracted light significantly.

Fig. 4 (c) shows comparisons with DDA [35] (black lines) of beam tracer results for P_{22}/P_{11}. Again, the green lines represent results obtained by Karczewski and Wolf's method [26], without application of the *VOF*. There is an overall agreement in shape, with values close to 1 in close to direct forward and backscattering and a minimum around 120˚ and a shoulder at about 60˚, however the beam tracer strongly overestimates the variation of P_{22}/P_{11} with scattering angle. This trend increases with decreasing size parameter. Including the *VOF* (blue lines) improves the results, however there is still a fairly large deviation from the DDA results. It was found that this overestimation of cross-polarisation is linked to the amplitude matrix for diffracted light derived in [26] using the Kirchhoff approximation. Cross polarisation is caused by the [1,2] and [2,1] elements of the matrices $\mathbf{S_D}$ and $\mathbf{S_R}$. We introduce a cross polarisation factor obtained as a fit function

$$CPF(X,\vartheta) = q(X)\,|\sin^3(\vartheta)|, \tag{6a}$$

where ϑ is the angle between the direction of observation and the respective geometric optics ray, i.e. the incident ray for external diffraction and the reflected ray for external reflection. Using the method of least squares a fit factor

$$q(X) = -0.6359\exp\left(-\frac{X}{60.2777}\right) + 0.7452 \tag{6b}$$

was obtained (Fig. 3b). The variation of the fit values for q with particle orientation for fixed size parameter was found to be small. It is assumed that q depends on the beam facing facet size and orientation rather than the shape and orientation of the whole particle, and that *CPF* approaches one for large size parameters and near perpendicular incidence. Results are shown as red lines in Fig. 4 (c), and also (a) and (b). The effect of the *CPF* on the phase function is negligible. $-P_{12}/P_{11}$ is slightly increased in the side scattering region.

Fig. 5 shows the average over the three investigated orientations of the azimuthally averaged P_{11}, $-P_{12}/P_{11}$ and P_{22}/P_{11} elements of the phase matrix.

We have demonstrated here, how studying the interrelation between different elements of the scattering matrix for absorbing particles can be used to improve the modelling of external diffraction and reflection. The deviation of scattering from modelling results obtained from the (*e*,*m*) theory [26] will increase towards side scattering (see analogous discussion for scalar diffraction theory in [42]). The *volume obliquity* factor *VOF* increases with increasing size parameter, affecting scattering most for large size parameters (eq. (5a)), i.e. large particle volumes obstructing external diffraction. The cross polarisation factor *CPF* also increases with size parameter, meaning that it affects scattering most for small size parameters (eq. (6a)).

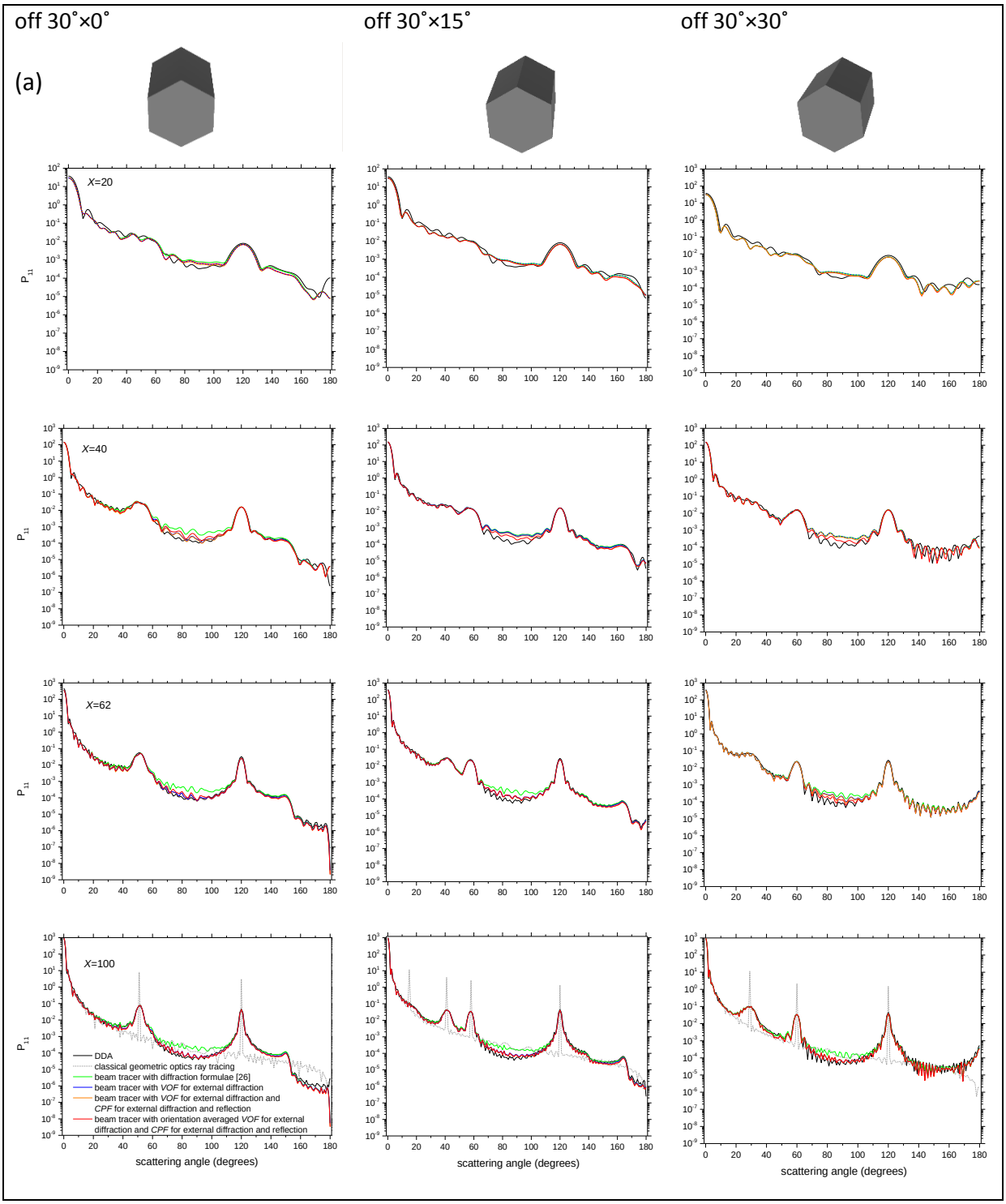

Fig.4 Azimuthally averaged elements of the phase matrix for a smooth hexagonal prism of refractive index 1.31 + 0.1i with an edge length a of the basal facets and a prism height 2 a for size parameters $X = 2\,\pi a / \lambda$ = 20, 40, 62 and 100 computed with DDA (black line), beam tracer with diffraction formulae [26] (green line), with *VOF* for external diffraction (blue line), with *VOF* for external diffraction and *CPF* for external diffraction and reflection (orange line) and with orientation averaged *VOF* and *CPF* (red line). (**a**) P_{11} (for X = 100 additionally classical geometric optics results are shown (gray line)), (b) $-P_{12}/P_{11}$, (c) P_{22}/P_{11}.

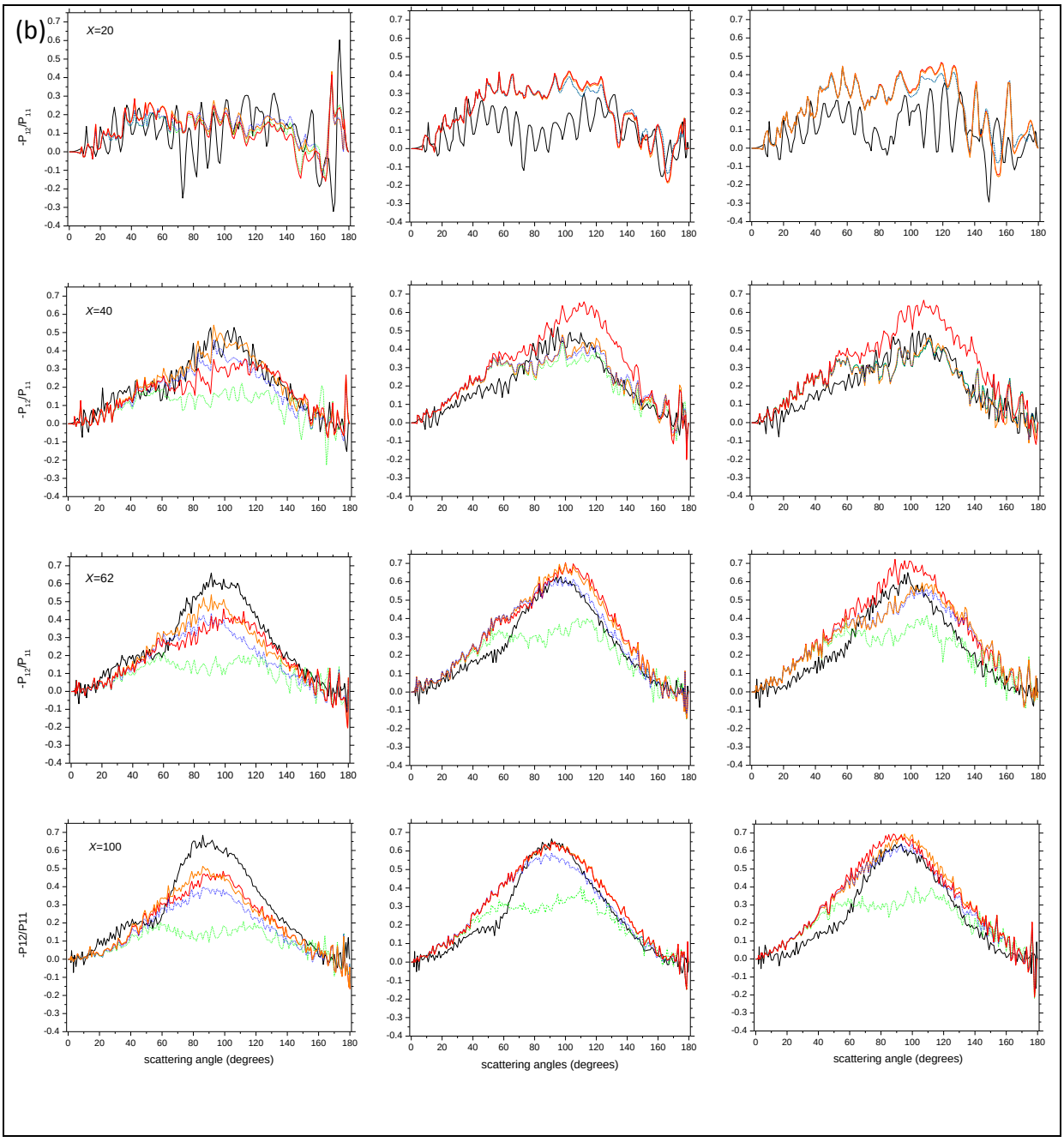

Fig.4 Azimuthally averaged elements of the phase matrix for a smooth hexagonal prism of refractive index 1.31 + 0.1i with an edge length a of the basal facets and a prism height 2 a for size parameters $X = 2\,\pi a / \lambda$ = 20, 40, 62 and 100 computed with DDA (black line), beam tracer with diffraction formulae [26] (green line), with *VOF* for external diffraction (blue line), with *VOF* for external diffraction and *CPF* for external diffraction and reflection (orange line) and with orientation averaged *VOF* and *CPF* (red line). (a) P_{11} (for X = 100 additionally classical geometric optics results are shown (gray line)), (**b**) $-P_{12}/P_{11}$, (c) P_{22}/P_{11}.

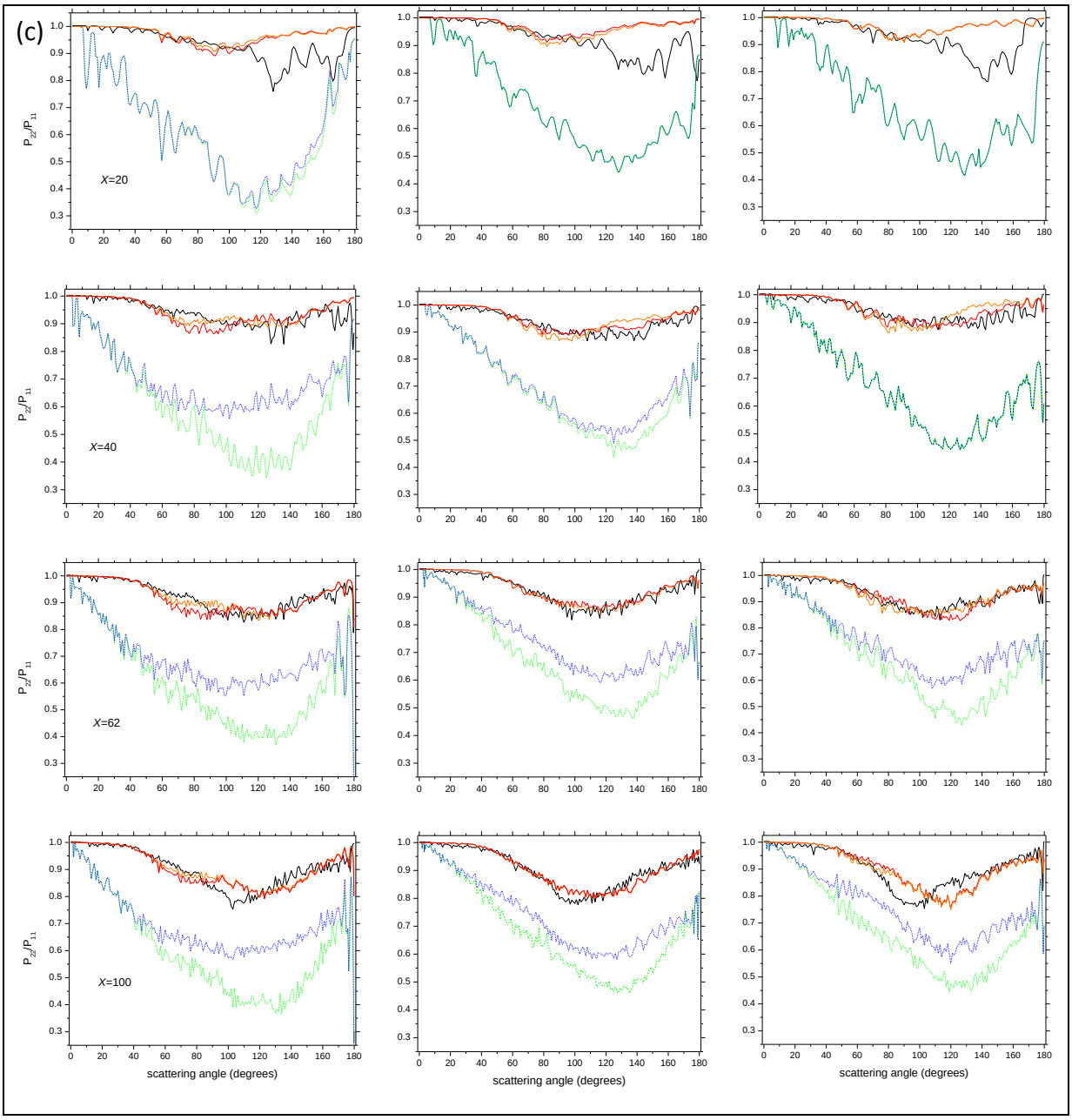

Fig.4 Azimuthally averaged elements of the phase matrix for a smooth hexagonal prism of refractive index 1.31 + 0.1i with an edge length a of the basal facets and a prism height 2 a for size parameters $X = 2\,\pi a / \lambda$ = 20, 40, 62 and 100 computed with DDA (black line), beam tracer with diffraction formulae [26] (green line), with *VOF* for external diffraction (blue line), with *VOF* for external diffraction and *CPF* for external diffraction and reflection (orange line) and with orientation averaged *VOF* and *CPF* (red line). (a) P_{11} (for X = 100 additionally classical geometric optics results are shown (gray line)), (b) $-P_{12}/P_{11}$, (**c**) P_{22}/P_{11}.

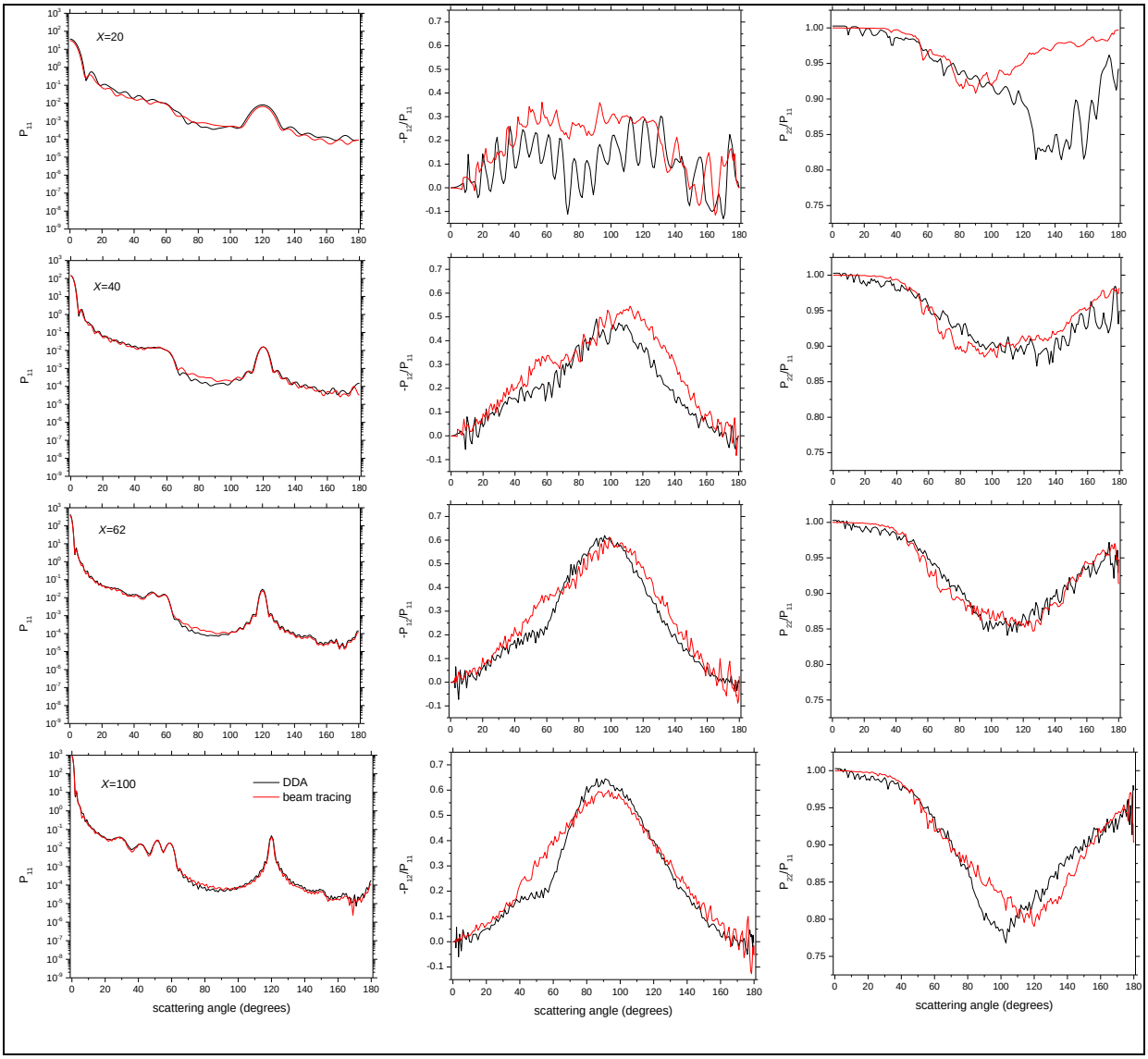

Fig. 5. Average over the three investigated orientations of the azimuthally averaged P_{11}, $-P_{12}/P_{11}$ and P_{22}/P_{11} elements of the phase matrix for a smooth hexagonal prism of refractive index 1.31+0.1i prism with an edge length a of the basal facets and a prism height $2a$ for size parameters $X = 2\pi a/\lambda$ = 20, 40, 62 and 100 computed with DDA (black line) and beam tracer with *VOF* for external diffraction and *CPF* for external diffraction and reflection (red line).

2.2 Application to slightly rough absorbing hexagonal prisms

Next, we investigate the applicability of this method to a slightly rough hexagonal prism with edge length 5 µm of the basal facets and a prism height 10 µm at a wavelength of 0.5 µm (size parameter 62). The construction of the rough crystal model is described in [41]. The Gaussian random surface has a standard deviation of 0.1 µm and a correlation length of 0.5 µm - see top of Fig. 6 for a visual representation of the particle. The average surface element (facet) size is 0.412 times the wavelength.

Since external diffraction is essentially determined by the particle contour, we compute it as diffraction by a smooth prism with the same overall dimensions [22], but include the factors *VOF* and *CPF* from section 2.1. External reflection is computed including the factor *CPF*. Contributions into any direction are obtained by summation of the reflection amplitude matrices for all beam-facing facets positioned on beam-facing parent facets [41] (i.e. basal or prism facets). Since the slight differences in 3D contour between the smooth and rough prism affect phase, external reflection and diffraction intensities (not amplitudes) are added.

The phase functions obtained by the beam tracer in this way are represented by blue lines in the first row of Fig. 6. They agree well with DDA (black lines), in particular for the orientation 'off 30˚×0˚'. For the other two orientations, P_{11} is slightly too high in the angular regions linked to reflections from prism facets labelled 1 and 3 in the upper row of Fig. 6 (15˚ and 43˚ for 'off 30˚×15˚', and 28˚ for 'off 30˚×30˚'), and in side scattering. We assume that this is due to not considering shadowing, which will increase with obliqueness of incidence and should be strongest for facet 3 in orientation 'off 30˚×15˚'. To address this problem, we have designed a method where the incident beam is divided into sub-beams with equilateral triangular cross sections. The intersection points of the three beam edges with the prism define the vertices of a triangle, which is treated as an incident-facing 'facet' by the beam tracer. In this way, we make sure that incidence-facing but shadowed crystal facets or regions thereof do not contribute to the phase functions, the results are represented by red lines in Fig. 6. In order to faithfully represent the crystal surface for the light scattering problem, a beam edge length of 0.125 µm (corresponding to a beam edge to wavelength ratio of 0.25) was chosen. This new method results in improved phase functions, in particular in the side scattering region. For comparison, Fig. 6 shows also results obtained by classical geometric optics (i.e. ray-tracing combined with Fraunhofer diffraction at the projected cross section, gray lines). Compared to the other methods, the reflection peaks, in particular in the forward scattering hemisphere, are much smoothed out. This is due to the fact that ray-tracing does not include phase and externally reflected light does not undergo diffraction. The latter also causes scattering in the region between 160˚ and 180˚ to be too low. Comparisons of 2D patterns with DDA are given in Fig. 7 (a). We find good agreement of the beam tracer results with DDA - note in particular the agreement in shape of the centres of the reflection peaks.

Azimuthally averaged $-P_{12}/P_{11}$ and P_{22}/P_{11} and the respective 2D patterns are shown in the 2nd and 3rd row of Fig. 6 and in Fig. 7 (b) and (c) respectively. Note that the maximum of $-P_{12}/P_{11}$ in side scattering for the DDA results is even higher than for the smooth prisms (Fig. 4(b)) and is shifted towards lower angles (centred around 80˚). This is most likely due to even more reflected light being scattered into the sideward region. The shift occurs in the beam tracer results too, however the peak height does not increase. The 2D patterns of $-P_{12}/P_{11}$ obtained from both, DDA and the beam tracer, show low linear polarisation arcs spreading from the centre in the forward scattering hemisphere, which can be linked to external diffraction. They are surrounded by a ring-shaped high linear polarisation area in side scattering, followed by a low linear polarisation area towards direct backscattering.

P_{22}/P_{11} deviates less from 1 than for the smooth prism, a trend shown by the beam tracer results, too. It is probably also linked to the wider angular distribution of reflected light caused by the particle roughness: The regions where P_{22}/P_{11} is low, i.e. the angle ϑ between the geometric optics ray and direction of observation is close to 90˚ (see eq. (6a)), spread out. For example, in Fig. 7(c) the speckle with low P_{22}/P_{11} on the backscattering hemisphere can be thought of being positioned on a ring centred at the 120˚ reflection peak, which changes position with particle orientation.

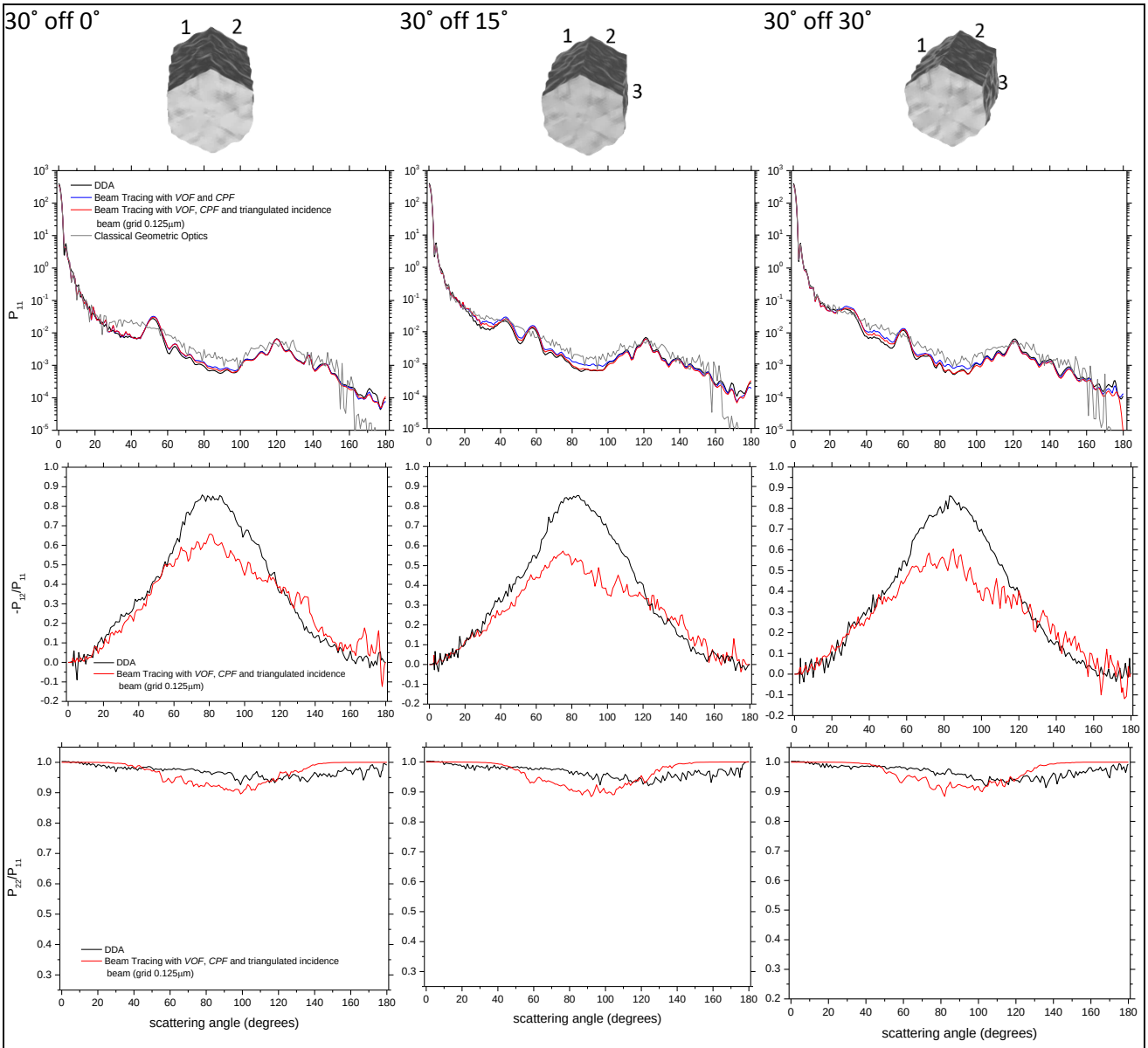

Fig. 6. Top: Orientations of the rough hexagonal prism of size parameter 62. Light incidence is perpendicular into the page. 1st row: Azimuthally averaged P_{11} computed with DDA (black line), beam tracing with *VOF* and *CPF* (blue line), beam tracing with *VOF, CPF* and triangulated incidence beam of edge length 0.125 μm (red line), and classical geometric optics (gray line), 2nd and 3rd row: Azimuthally averaged $-P_{12}/P_{11}$ and P_{22}/P_{11}, respectively, computed with DDA (black line), beam tracing with *VOF*, *CPF* and triangulated incidence beam of edge length 0.125 μm (red line).

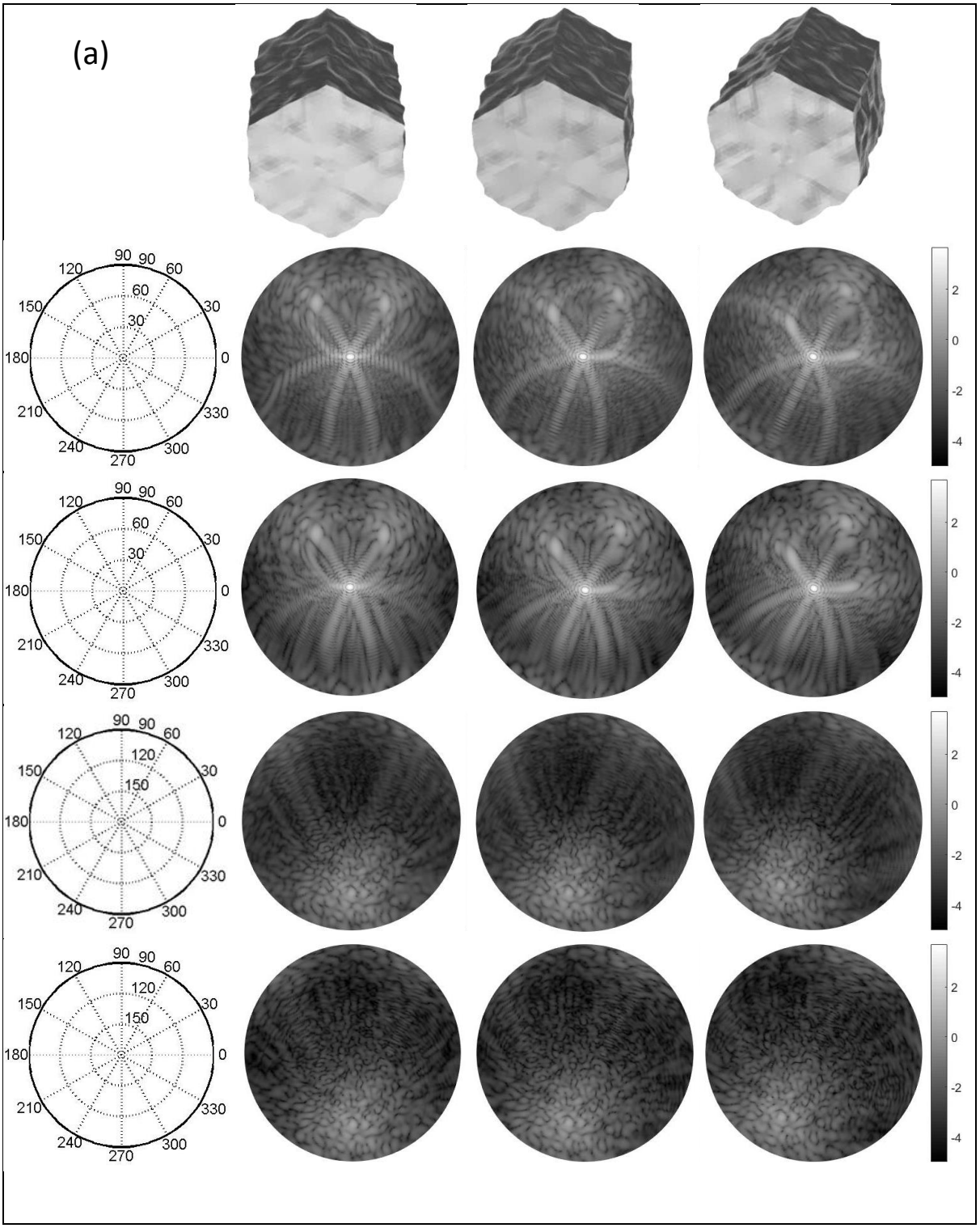

Fig. 7. 2D patterns of phase matrix elements for a hexagonal prism of size parameter 62 with Gaussian random surface (correlation length 0.5 μm, standard deviation 0.1 μm, average facet dimension is 0.412 times the wavelength) obtained by beam tracing with *VOF* , *CPF* and triangulated incidence beam (edge length 0.125 μm). Shapes and orientations are shown on top of the figure. DDA results are presented in rows 2 and 4, and beam tracing results in rows 1 and 3. Results for the forward scattering hemisphere are shown in rows 1 and 2, and results for the backscattering hemisphere in rows 3 and 4. (**a**) P_{11} , (b) $-P_{12}/P_{11}$, (c) P_{22}/P_{11}.

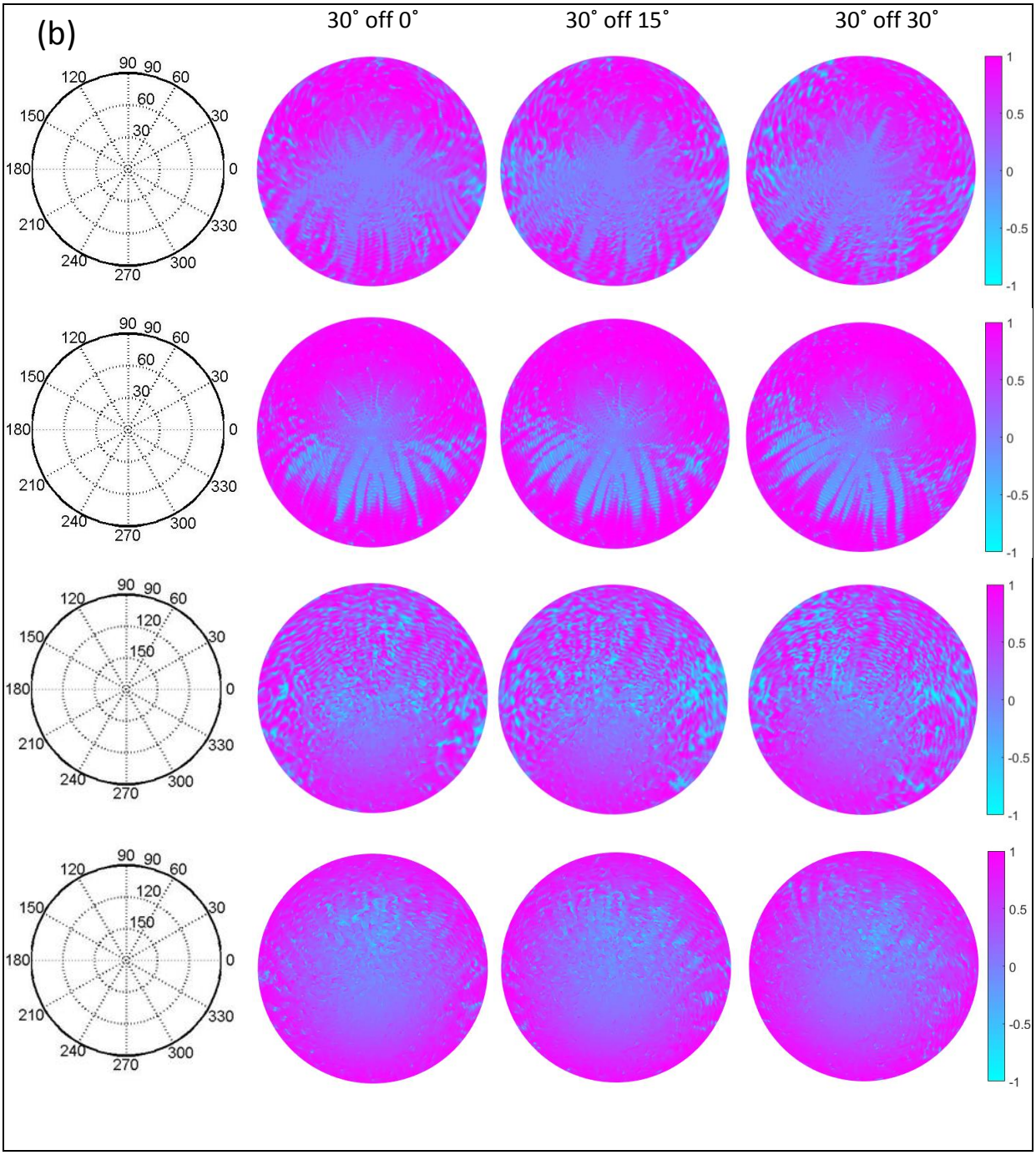

Fig. 7. 2D patterns of phase matrix elements for a hexagonal prism of size parameter 62 with Gaussian random surface (correlation length 0.5 µm, standard deviation 0.1 µm, average facet dimension is 0.412 times the wavelength) obtained by beam tracing with *VOF* , *CPF* and triangulated incidence beam (edge length 0.125 µm). Shapes and orientations are shown on top of the figure. DDA results are presented in rows 2 and 4, and beam tracing results in rows 1 and 3. Results for the forward scattering hemisphere are shown in rows 1 and 2, and results for the backscattering hemisphere in rows 3 and 4. (a) P_{11} , (**b**) $-P_{12}/P_{11}$, (c) P_{22}/P_{11}.

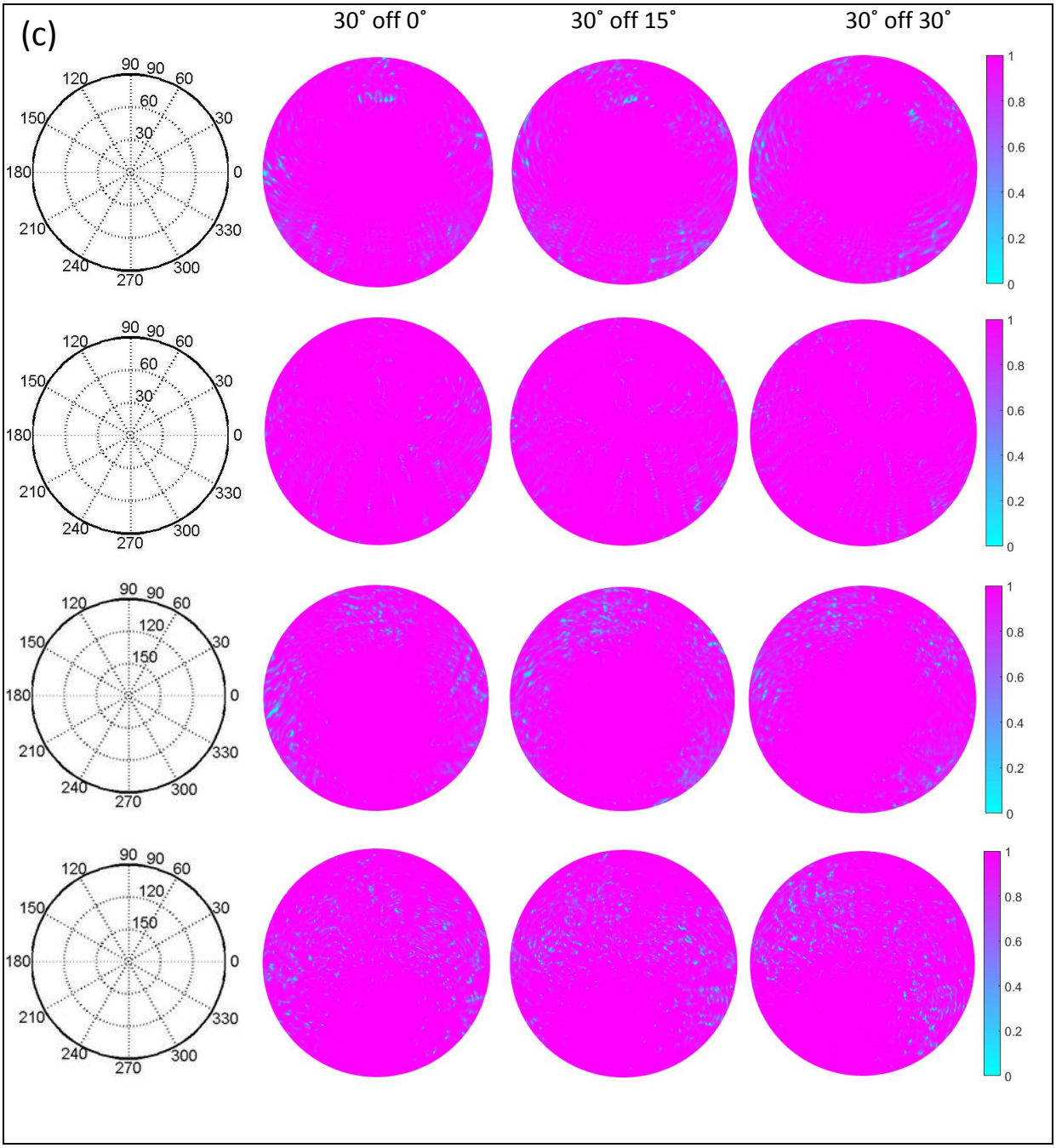

Fig. 7. 2D patterns of phase matrix elements for a hexagonal prism of size parameter 62 with Gaussian random surface (correlation length 0.5 µm, standard deviation 0.1 µm, average facet dimension is 0.412 times the wavelength) obtained by beam tracing with *VOF* , *CPF* and triangulated incidence beam (edge length 0.125 µm). Shapes and orientations are shown on top of the figure. DDA results are presented in rows 2 and 4, and beam tracing results in rows 1 and 3. Results for the forward scattering hemisphere are shown in rows 1 and 2, and results for the backscattering hemisphere in rows 3 and 4. (a) P_{11} , (b) $-P_{12}/P_{11}$, (**c**) P_{22}/P_{11}.

3. Conclusions

The (*e*) and (*m*) methods, which were proposed by Karczewski and Wolf [26] as alternatives to the (*e,m*) method for their vector diffraction approximation, link reflection from metals with external diffraction. This can be explained by the particular choice of boundary conditions, which assume

continuity of the tangential component for either **E** or **H** field and disregard the other field component, which effectively is a boundary condition for a conductor, at least for the **E**-field. Our results have confirmed that only the (*e,m*) method is suitable for computing external diffraction and diffraction of externally reflected beams.

The application of the beam tracing method to strongly absorbing particles allowed us a closer investigation of the external diffraction component because transmission is negligible. To mitigate the slightly overestimated side scattering by three-dimensional objects computed by the beam tracer due to applying a physical optics model for two-dimensional apertures, a particle size dependent 'volume obliquity factor' $VOF(X,\theta)$ has been introduced. This factor has been estimated by investigating the case of a dielectric, strongly absorbing compact hexagonal prism for three particle orientations at four size parameters between 20 and 100. The resulting *VOF* improved the results for phase functions and $-P_{12}/P_{11}$, indicating that the approach is broadly correct (in this initial investigation the dependence on azimuthal angle has been neglected). The *VOF* would need to be generalised with respect to particle shape. Introducing the *VOF* improved beam tracer results for P_{22}/P_{11} as well, however there was still a noticeable deviation from the DDA results, in particular for small size parameters. To mitigate this overestimation of cross polarisation a size parameter dependent 'cross polarisation factor' $CPF(X,\theta)$ has been introduced. Note that the overestimation of side scattering without application of $VOF(X,\theta)$ will affect scattering results for transparent particles less, since more beam paths will contribute to the overall scattering pattern.

This method has been applied for computing light scattering by absorbing, slightly rough hexagonal prisms. Correct phase relationships between beams originating from different facets are essential. For particle orientations where shadowing is not negligible, phase functions can be improved by using a new method where the incident beam is divided into sub-beams with triangular cross sections. The intersection points of the three beam edges with the prism define the vertices of a triangle, which is treated as an incident facing facet by the beam tracer. This ensures that incident facing but shadowed crystal facets or regions thereof do not affect the phase matrix. 2D patterns of P_{11}, $-P_{12}/P_{11}$ and P_{22}/P_{11} have been computed. Good results for 2D scattering patterns and azimuthally averaged phase function in fixed orientation have been obtained. The method captures much of the fine detail contained in 2D scattering patterns. This is important as speckle can be used for characterizing the size [6] and roughness [5] of small particles such as ice crystals. Here, we have studied light scattering by absorbing particles, which allowed us to separately investigate the external diffraction and reflection contributions. This allowed the introduction of the volume obliquity factor and the cross polarisation factor. It is anticipated that such factors as well as the new sub-beam method are also applicable to transparent particles.

Acknowledgement

E. Hesse, L. Taylor, C.T. Collier and Z. Ulanowski acknowledge support by the Natural Environment Research Council, United Kingdom (Grant no. NE/I020067/1 (EH, ZU) and NERC Doctoral Training Programme no. NE/K50130X/1 (LT), NE/I528377/1 (CTC).

The DDA results have been computed using services by CSC, the Finnish IT Centre for Science.

Appendix

Rotation matrices have the general form [43]

$$\mathbf{R} = \begin{bmatrix} \cos\varphi & \sin\varphi \\ -\sin\varphi & \cos\varphi \end{bmatrix} \tag{7}$$

where φ is the angle by which the initial matrix is rotated counter clockwise.

The amplitude diffraction matrix for the (*e,m*) theory is given by

$$\mathbf{D} = F\begin{bmatrix} -\left(k_z\frac{\sqrt{1-K_y^2}}{\sqrt{1-k_y^2}} + K_z\frac{\sqrt{1-k_y^2}}{\sqrt{1-K_y^2}}\right) & \left(k_xk_y\frac{\sqrt{1-K_y^2}}{\sqrt{1-k_y^2}} - K_xK_y\frac{\sqrt{1-k_y^2}}{\sqrt{1-K_y^2}}\right) \\ \left(K_xK_y\frac{\sqrt{1-k_y^2}}{\sqrt{1-K_y^2}} - k_xk_y\frac{\sqrt{1-K_y^2}}{\sqrt{1-k_y^2}}\right) & -\left(K_z\frac{\sqrt{1-k_y^2}}{\sqrt{1-K_y^2}} + k_z\frac{\sqrt{1-K_y^2}}{\sqrt{1-k_y^2}}\right) \end{bmatrix} \quad (8)$$

where indices *xyz* indicate the components of the respective vector in *xyz*-coordinates.

References

[1] Baran A. A review of the light scattering properties of cirrus. J Quant Spectrosc Radiati Transf 2009;110:1239–60.

[2] Yu H, Kaufman YJ, Chin M, Feingold G, Remer LA, Anderson TL, et al. A review of measurement-based assessments of the aerosol direct radiative effect and forcing. Atm Chem Phys 2006;6:613–66.

[3] Baumgardner D, Abel S, Axisa D, Cotton R, Crosier J, Field PR, Gurganus C, Heymsfield AJ, Korolev A, Kraemer M, Lawson P, McFarquhar G, Ulanowski Z. & Um J. Cloud Ice Properties: In Situ Measurement Challenges. Meteor. Monogr. 2017;58, 9.1–9.23. 23 p.

[4] Kaye PH, Hirst E, Greenaway RS, Ulanowski Z, Hesse E, DeMott PJ, Saunders C, Conolly P. Classifying atmospheric ice crystals by spatial light scattering. Opt Lett 2008;33:1545–7.

[5] Ulanowski Z, Kaye PK, Hirst E, Greenaway RS, Cotton RJ, Hesse E, and Collier CT. Incidence of rough and irregular atmospheric ice particles from Small Ice Detector 3 measurements. Atmos Chem Phys 2014;14:1649–1662.

[6] Ulanowski Z, Hirst E, Kaye PH, Greenaway R. Retrieving the size of particles with rough and complex surfaces from two-dimensional scattering patterns. J Quant Spectrosc Radiat Transf 2012;113:2457-64.

[7] Mishchenko MI, Zakharova NT, Khlebtsov NG, Wriedt T, Videen G. Comprehensive thematic T-matrix reference database: A 2013-2014 update. J Quant Spectrosc Radiat Transf 2014;146, 349-354.

[8] Yang P, Liou KN. In: Mishchenko MI, Hovenier JW, Travis LD, editors. Light scattering by nonspherical particles. New York: Academic Press; 1999. p. 173–221.

[9] Yurkin MA, Maltsev VP, Hoekstra AG. The discrete dipole approximation: An overview and recent developments. J Quant Spectrosc Radiat Transf 2007;106:558–89.

[10] Muinonen K. Scattering of light by crystals: a modified Kirchhoff approximation. Appl Opt 1989;28:3044–50.

[11] Yang P, Liou KN. Geometric-optics-integral equation method for light scattering by nonspherical ice crystals. Appl Opt 1996;35:6568–84.

[12] Borovoi, AG, and Grishin, IA, Scattering matrices for large ice crystal particles, J. Opt. Soc. Am. A 20(2003), 2071-2080.

[13] Bi L, Yang P, Kattawar GW, Hu Y, Baum BA. Scattering and absorption of light by ice particles: solution by a new physical–geometric optics hybrid method. J Quant Spectrosc Radiat Transf 2011:1492–508.

[14] Yang P, Liou KN. Light scattering by hexagonal ice crystals: solutions by a ray-by-ray integration algorithm. J Opt Soc Am A 1997;14:2278-2289.

[15] Yang P, Gao B-C, Baum BA, Hu YX, Wiscombe WJ, Mishchenko MI, Winker DM, and Nasiri SL. Asymptotic solutions for optical properties of large particles with strong absorption. Appl Opt 2001; 40:1532-1547

[16] Bi L, Yang P, Kattawar GW, Hu Y, Baum BA. Diffraction and external reflection by dielectric faceted particles. J Quant Spectrosc Radiat Transf 2011;112:163-173.

[17] Macke A, Mueller J, Raschke E. Single scattering properties of atmospheric ice crystals. J Atm Sci 1996;53:2813–25.

[18] Macke A, Mishchenko MI. Applicability of regular particle shapes in light scattering calculations for atmospheric ice particles. Appl Opt 1996; 35(21): 4291-4296.

[19] Hesse E, Mc Call DS, Ulanowski Z, Stopford C, Kaye PH. Application of RTDF to particles with curved surfaces. J Quant Spectros Radiat Transf 2009:1599–603.

[20] Jackson JD. Classical electrodynamics. 3rd ed. New York: John Wiley & Sons; 1999.

[21] Hesse E, Macke A, Havemann S, Baran AJ, Ulanowski Z, Kaye PH. Modelling diffraction by facetted particles. J Quant Spectrosc Radiat Transf 2012:113, 342–347.
[22] Hesse E, Collier CT, Penttilä A, Nousiainen T, Ulanowski Z, Kaye PH. Modelling light scattering by absorbing smooth and slightly rough facetted particles. J Quant Spectrosc Radiat Transf 2015; 157:71–80.
[23] Taylor L, Hesse E, Pentillä A, Ulanowski Z, Nousiainen T, Kaye PH. A beam tracing model applied to transparent, smooth hexagonal columns. Comparisons to ADDA. (in preparation).
[24] Clarke AJM, Hesse E, Ulanowski Z, and Kaye PH. A 3D implementation of ray tracing combined with diffraction on facets: Verification and a potential application. J Quant Spectrosc Radiat Transf 2006;100:103-114.
[25] Goerke M, Ulanowski Z, Ritter G, Hesse E, Neely RR, Taylor L, Stillwell RA, and Kaye PH. Characterizing ice particles using two-dimensional reflections of a lidar beam. Appl Opt 2017;56:G186-G196.
[26] Karczewski B, Wolf E. Comparison of three theories of electromagnetic diffraction at an aperture. Part I: Coherence Matrices. J Opt Soc Am 1966;56:1207-1214.
[27] Karczewski B, Wolf E. Comparison of three theories of electromagnetic diffraction at an aperture. PartII: The far field. J Opt Soc Am 1966;56:1214–19 .
[28] Konoshonkin AV, Kustova NV, Borovoi AG, Grynko Y, Förstner J. Light scattering by ice crystals of cirrus clouds: comparison of the physical optics methods. J Quant Spectrosc Radiat Transf 2016;182:12-23.
[29] Bi L, Yang P, Kattawar GW, and Kahn R. Single-scattering properties of triaxial ellipsoidal particles for a size parameter range from the Rayleigh to geometric-optics regimes. Appl Opt 2009;48:114-126.
[30] Shcherbakov V, Gayet J-F, Baker BA, Lawson RP. Light scattering by single natural ice crystals. J. Atmos. Sci. 2006, 63, 1513-1525.
[31] Baum BA, Yang P, Heymsfield AJ, Schmitt CG, Xie Y, Bansemer A, Hu YX, and Zhang Z. Improvements in shortwave bulk scattering and absorption models for the remote sensing of ice clouds, J App. Metero. Clim 2011;50:1037–1056.
[32] Yang P and Liou KN. Single-scattering properties of complex ice crystals in terrestrial atmosphere. Contr Atmos Phys 1998;71:223-248.
[33] Liu C, Panetta RL, Yang P. The effects of surface roughness on the scattering properties of hexagonal columns with sizes from the Rayleigh to the geometric optics regimes. J Quant Spectrosc Radiat Transf 2013;129:169-185.
[34] Baum, BA, Yang, P, Hu, YX, Feng, Q. The impact of ice particle roughness on the scattering phase matrix. J Quant Spectrosc Radiat Transf 2010;111:2534-49.
[35] Yurkin MA, Hoekstra AG. The discrete-dipole-approximation code ADDA: capabilities and known limitations. J Quant Spect Rad Trans 2011;112:2234–47.
[36] Macke A. Modellierung der optischen Eigenschaften von Cirruswolken. PhD thesis. Germany: University of Hamburg; 1994.
[37] Di Francia GT. Electromagnetic Waves. New York: lnterscience Publishers Inc; 1955 (chapter 10).
[38] Kuper TG, Shack RV. Decompositions in vector diffraction theory. Proc. SPIE 1985;560:2-11.
[39] Johnson PB and Christy RW. Optical constants of the noble metals. Phys Rev B 1972;6:4370-4379.
[40] Born M, Wolf E. Principles of optics, 7th ed. Cambridge: CUP, 1999 (chapter10.2).
[41] Collier CT, Hesse E, Taylor L, Ulanowski Z, Penttilä A, Nousiainen T. Effects of surface roughness with two scales on light scattering by hexagonal ice crystals large compared to the wavelength: DDA results. J Quant Spectrosc Radiat Transf 2016;182:225-39.
[42] Ogilvy JA. Accuracy of Kirchhoff theory. Chapter4.2. In: Theory of wave scattering from random rough surfaces. Bristol: Adam Hilger; 1991.
[43] Hovenier, JW, Mee, CVM. Fundamental relationships relevant to the transfer of polarized light in a scattering atmosphere. Astron. Astrophys. 1983;128:1-16.